24th COBEM - 2017

24th ABCM International Congress of Mechanical Engineering
December 3-8, 2017, Curitiba, PR, Brazil

COBEM-2017-0917
ON THE USE OF HEAT EXCHANGE´S DEVICES IN ORDER TO IMPROVE ADSORPTION AND DESORPTION PROCESS OF ANG TANKS

Bruno Galelli Chieregatti
João de Sá Brasil Lima
Ernani Vitillo Volpe
Marcelo Tanaka Hayashi
Research Centre for Gas Innovation, Escola Politécnica da Universidade de São Paulo (EPUSP), Av. Prof Mello Moraes, 2231, CEP: 05508-000
bchieregatti@usp.br; jblima@usp.br; ernvolpe@usp.br; mthayashi@gmail.com

Abstract. *In recent years, the Adsorbed Natural Gas (ANG) technology has been identified as the most promising low-pressure alternative for storing natural gas. Although ANG does not attain the same capacity of liquefied natural gas (LNG) systems, it provides a method for storing gas at substantially higher concentration than can be achieved with simple compression (Compressed Natural Gas - CNG), and dismiss the use of refrigeration. One important issue on the use of this technology is to improve the adsorption (filling) and desorption (deflation) processes. This is achieved by increasing the relation between the volume of stored gas at ambient conditions and the volume of the tank (known as V/V). Due to the physics of the process, the gas temperature increases during adsorption, hence it decreases the adhesion of molecules to the adsorbent. The opposite occurs in the desorption process, when the temperature decreases, thus making it more difficult to release the gas. In order to improve these processes, this work focuses on the use of heat exchanger devices. To show the influence of these devices on the processes, numerical transient 2D axi-symmetric simulations are carried out, by using a finite-element platform FreeFEM++, and on considering that the flow is governed by Navier-Stokes equations, ruled by Darcy's law. For each test case, the V/V relation and the mass of gas will be calculated and compared, to show the influence of the devices. This article is a project from the Research Centre for Gas Innovation (RCGI), which started in 2016, with support from BG Shell and FAPESP.*
Keywords: *Adsorption, Natural Gas, Storage Vessels, Heat Exchangers*

1. INTRODUCTION

In the beginning of the 21th century, the Natural Gas (NG) is considered one of the most important energy sources worldwide. According to most recently published data (CIA , 2016) , the reserves are estimated at almost 180 trilions of cubic meters. However, they are not homogeneously distributed around the globe, and the consumption shows the same behavior. The demand sustains an important bilionary market around the world and the basic structure of this market involves several stages:

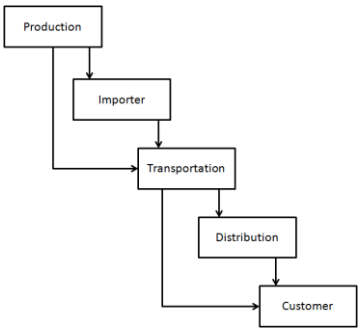

Figure 1: NG market basic structure

This article focuses on the transportation stages and, in particular, on storage vessels. Nowadays, the Transportation companies have two different technologies to deliver NG without pipelines:

- Compressed Natural Gas (CNG): The simplest way to store NG. It consists of a tank (cylinder or sphere) that receives NG through a compressor. Pressures range from as low as 10 bar up to 200 bar.

- Liquefied Natural GAS (LNG): This technology is more complex than CNG. Because it involves a cryogenics procedure. The Methane boiling point is close to 112K at atmosphere pressure and LNG involves liquefying NG to increase its specific volume, while keeping the pressure lower than CNG technology.

In the present scenario, the Adsorbed Natural Gas technology (ANG) has become an attractive alternative for storage systems. The method provides a means of storing gas at substantially higher concentration than can be achieved with CNG at the same pressure. Although it does not attain the density that is typically found with LNG, it is potentially much simpler, since it does not require the energy-demanding liquefaction process (Judd, 1998). Qualitatively, the following table presents common pressures, temperatures and V/V, defined as volume of gas stored divided by internal tank volume under STP conditions, for the types of transportation technologies:

Table 1 – Comparison between transport technologies (Hirata, 2009)

	Pressure (bar)	Temperature (°C)	V/V
CNG	200	-15 to 40	200
LNG	1	-163	600
ANG	35-50	-15 to 40	150-180

The V/V parameter is one of most important metrics to qualify the ANG Storage tanks. To show its importance, the U.S. Department of Energy (US-DOE) sets a target of 180 V/V at 35 bar and ambient temperature as the point when ANG become a viability alternative. To achieve this target, some adsorbents are developed with good adsorption capacity and high packing density for the ANG storage applications (Rahman, 2011). However, it is not only about developing new adsorbent materials. The ANG technology, itself, needs improvements, so as to keep pace with the new, improved, materials. It is important to point out that the development of new adsorbent materials is not the scope of this article. This work is focused on numerical simulations using existent or developed adsorbents and the objective is to improve the heat transfer process during the filling procedure.

2. MATHEMATICAL MODEL

The governing equations which modeled a flow through a porous media with adsorption are presented below, where the main assumptions are: Pure NG (100% Methane as ideal gas); properties of the adsorbent bed are constant and the bed is considered isotropic with spherical particles and homogenous pores distribution (Sahoo,2011):

$$\epsilon_t \frac{\partial \rho_g}{\partial t} + \rho_b \frac{\partial q}{\partial t} + \nabla . \vec{G} = 0 \quad (1)$$

$$\rho_g \nabla p + \frac{\mu}{K} \vec{G} = 0 \quad (2)$$

$$C_{eff} \frac{\partial T}{\partial t} - \epsilon_t \frac{\partial p}{\partial t} + \nabla . \left(C_{pg} \vec{G} T\right) - \lambda_{eff} \nabla^2 T - \frac{\Delta H}{M_g} \rho_b \frac{\partial q}{\partial t} = 0 \quad (3)$$

$$q = \rho_{ads} . W_0 . exp\left[-\left(\frac{A}{\beta E_0}\right)^n\right] \quad (4)$$

Equation (1) is the continuity equation where ϵ_t is the total porosity of adsorbent bed (no-dimensional); ρ_g is the free gas density (located in the voids between particles and in the respective pores); ρ_b is the density of adsorbent bed; q is the density of adsorption, which is given by the eq. (4) and $\vec{G}$ is the specific mass flux vector, defined by $\vec{G} = \rho . \vec{u}$.
Equation (2) are the momentum equations (2D axi-symmetric) with Darcy law simplifications, where ∇p is the pressure gradient; μ is the gas viscosity, and K is the permeability of the adsorbent bed (m²), given in terms of porosity and the average radius of the adsorbent particles [4].
Equation (3) is the Energy equation, where $C_{eff} = \left(\epsilon_t \rho_g + \rho_b q\right) C_{pg} + \rho_b C_{ps}$, which C_{pg} and C_{ps} represents the specifics heat of gas and adsorbent respectively; T represents the temperature; $\lambda_{eff} = \epsilon_t . \lambda_g + (1 - \epsilon_t) \lambda_s$ is the effective thermal conductivity in terms of porosity and thermal conductivity of gas(λ_g) and adsorbent (λ_s), ΔH is the heat of adsorption which is assumed constant and M_g is the molar mass of the gas.
Finally, eq. (4) is the Dubinin-Astakov (D-A) adsorption model (Sahoo,2011; Mota, 1995), where ρ_{ads} is the adsorbed gas density, defined by: $\rho_{ads} = \frac{\overline{\rho_{ads}}}{\exp[\alpha_e (T - T_b)]}$, where $\overline{\rho_{ads}}$ is the density of liquid phase of the adsorbed fluid in the saturation region (T_b) and α_e is the mean value of the thermal expansion of the liquefied gas, W_0 is the microporous volume per unit mass of adsorbent, β is the affinity coefficient related to the adsorbate-adsorbent interaction, E_0 is the characteristic energy of adsorption, and n is the DA exponent which is related to the pore size dispersion (Sahoo,2011). The variable A is the so-called as Polany adsorption potential and it is defined by: $A = RTln\left(\frac{P_s}{P}\right)$, where $P_s = P_{cr}\left(\frac{T}{T_{cr}}\right)^2$.

Before the numerical implementation of the equations (1) to (4), all of them were nondimensionalized, to avoid bad conditioning of matrices that are used to solve the flow equations numerically. The dimensionless variables (with *) are scaled to a fixed reference state:

$$t^* = t\frac{v_\infty}{l_{ref}} \qquad \rho^* = \frac{\rho}{\rho_\infty} \qquad p^* = \frac{p}{p_\infty}$$
$$T^* = \frac{T}{T_\infty} \qquad \vec{G}^* = \frac{\vec{G}}{\rho_\infty v_\infty} \qquad C_{px}^* = \frac{C_{px}}{C_{pg}} \qquad (5)$$
$$C_{eff}^* = \frac{C_{eff}}{\rho_\infty C_{pg}} \qquad \Delta H^* = \frac{\Delta H}{\rho_\infty C_{pg} T_\infty l_{ref}^3} \qquad M_g^* = \frac{M_g}{\rho_\infty l_{ref}^3}$$

where l_{ref} is the reference length and ρ_∞, p_∞ and T_∞ are, respectively, density, pressure and temperature of the reference state. Hence, the set of non-dimensional equations is given below. The symbol "*" was suppressed for convenience and, from now on, all variables presented are dimensionless. Additionaly, the non dimensional ideal gas equation ($p = \rho T$) was used, to solve the equations in terms of $p, \vec{G}, T$ *and* q:

$$\epsilon_t\left(\frac{1}{T}.\frac{\partial p}{\partial t} + \frac{p}{T^2}.\frac{\partial T}{\partial t}\right) + \rho_b\frac{\partial q}{\partial t} + \nabla.\vec{G} = 0 \qquad (6)$$

$$\vec{G} + N_p\rho_g\nabla p = 0 \qquad (7)$$

$$C_{eff}\frac{\partial T}{\partial t} - \epsilon_t\left(\frac{\gamma-1}{\gamma}\right)\frac{\partial p}{\partial t} + \nabla.\left(\vec{G}.T\right) - \frac{1}{Pe}\nabla^2 T - \frac{\rho_b\Delta H}{M_g}.\frac{\partial q}{\partial t} = 0 \qquad (8)$$

$$q = \rho_{ads}.W_0.exp\left[-\left(\frac{A}{\beta E_0}\right)^n\right] \qquad (9)$$

Where $N_p = \frac{K\rho_\infty}{\mu l_{ref} v_\infty}$ is the pressure number and $P_e = \frac{\rho_\infty C_{pg} v_\infty l_{ref}}{\lambda_{ref}}$ is the Péclet number.

3. NUMERICAL IMPLEMENTATION

The equations were implemented in FREEFEM++ platform (Hecht, 2012). This software is a high level integrated development environment for numerically solving partial differential equations in 2 and 3 dimensions. To simulate the above equations, it is necessary to define a set of boundary conditions. The set is presented below:

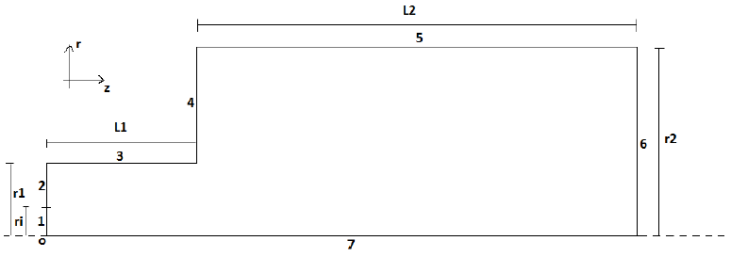

Figure 2. Schematic of a ANG Storage System – The point "o" represents the origin of coordinate system.

Table 2 – Set of Boundary Conditions

Boundary	Conditions
Inflow (Section 1): Parabolic mass flux in the axial direction.	$G_z = 2\left(\frac{\rho_0}{\rho_\infty}\right)\left(\frac{u_{in}}{u_\infty}\right)\left(1 - \frac{r^2}{r_i^2}\right)$, $G_r = 0$ $T = \frac{T_{inlet}}{T_\infty}$
Wall (Sections 2 to 6): No slip boundary condition with heat transfer	$G_z = 0$, $G_r = 0$ $-n.\nabla T = N_u(T - T_{ext})$
Symmetry (Section 7): Since the symmetry axis is parallel to z axis, the condition $\vec{G}.\vec{n} = 0$ reduces to $G_r = 0$.	$G_r = 0$ $n.\nabla T = 0$

where ρ_0 is the density of the gas in the inlet; u_{in} is the velocity based on volumetric flow rate at STP in section (1); T_{ext} is the ambient air temperature and N_u is the Nusselt number defined as $N_u = \frac{h.l_{ref}}{\lambda_{eff}}$

4. VALIDATION TESTS

Here the numerical implementation was validated. To use Galerkin's formulation one define an inner product $< f, g >= \int_\Omega f.g\, dV$ and the generic weight functions for Mass, Momentum, Energy and Adsorption equations ($p_w, \vec{v} = (v_r, v_z), t_w \; and \; q_w$). Now, one can apply the volume integration to the equations:

$$< \epsilon_t \left(\frac{1}{T}.\frac{\partial p}{\partial t} + \frac{p}{T^2}.\frac{\partial T}{\partial t}\right), pw > + < \rho_b \frac{\partial q}{\partial t}, pw > + < \nabla.\vec{G}, pw > = 0 \quad (10)$$

$$< \vec{G}, \vec{v} > + < N_p \rho_g \nabla P, \vec{v} > = 0 \quad (11)$$

$$< C_{eff}\frac{\partial T}{\partial t}, tw > - < \epsilon_t \left(\frac{\gamma-1}{\gamma}\right)\frac{\partial p}{\partial t}, tw > + < \nabla(\vec{G}.T), tw > - < \frac{1}{Pe}\nabla^2 T, tw > + \\ - < \frac{\rho_b \Delta H}{M_g}.\frac{\partial q}{\partial t}, tw > = 0 \quad (12)$$

For Adsorption model we have:

$$< q - \rho_{ads}.W_0.\exp\left[-\left(\frac{A}{\beta E_0}\right)^n\right], qw > = 0 \quad (13)$$

After the equations were implemented into FREFEEM++, we have to carry out validation tests, to check if the model could reproduce results that are presented in the literature. We choose to compare our results to those that are presented in [4]. Because not only do the authors show numerical simulations, but they also discuss experimental results. The basic tank dimensions are presented in the table below:

Table 3 – Tank Dimensions (based on Figure 2) – Same of presented in (Sahoo,2011). The internal volume is 1.82 L

Parameter	Value (mm)
Inlet Radius (ri)	3.175
Inlet Head Radius (r_1)	13.000
Tank Radius (r_2)	53.300
Inlet Head lenght (L_1)	30.000
Tank lenght (L_2)	202.000

The FREEFEM++ mesh generator is a suitable tool and it was used to generate a 490 triangle elements mesh, with specific refinements at the inlet region. The following figure depicts the mesh geometry chosen after a mesh sensitivity analysis:

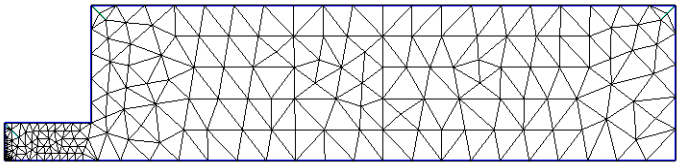

Figure 3. Mesh Generated by FREEFEM++

The next table presents the values that are used in the simulation setup:

Table 4 – Data and Initial Conditions – Same of presented in [4]

	Value		Value		Value
ρ_0	$0.7049\ kg/m^3$	T_∞	$300\ K$	α	$2.5\ e-03\ K^{-1}$
C_{pg}	$2450\ J/kg.K$	C_{ps}	$650\ J/kg.K$	E_0	$25.04\ e+03\ J/mol$
μ_g	$1.25\ e-05\ Pa.s$	λ_g	$0.0343\ W/m.K$	P_{cr}	$45.96\ e+05\ Pa$
ϵ_t	0.65	ϵ_b	0.30	$\overline{\rho_{ads}}$	$422.62\ kg/m^3$
λ_s	$0.54\ W/m.K$	ρ_b	$500\ kg/m^3$	n	1.8
ΔH	$12000\ J/mol$	h	$5\ W/m^2K$ (natural)	β	0.35
M_g	$0.016\ kg/mol$		$700\ W/m^2K$ (forced)	W_0	$3.3\ e-04\ m^3/kg$
		K	$3.7\ e-10\ m^2$	T_{cr}	$191\ K$
* STP Conditions		P_i	$20000\ Pa$	T_b	$111.2\ K$
		T_i	$303\ K$	k	$3.2\ s^{-1}$
		q_i	$q(P_i, T_i)$		

The following figures represent the evolution of the maximum temperature and the average pressure during the filling process. Two volumetric flow rates were tested: $10\ L/min$ and $30\ L/\min(STP)$. External natural convection were imposed on these simulations:

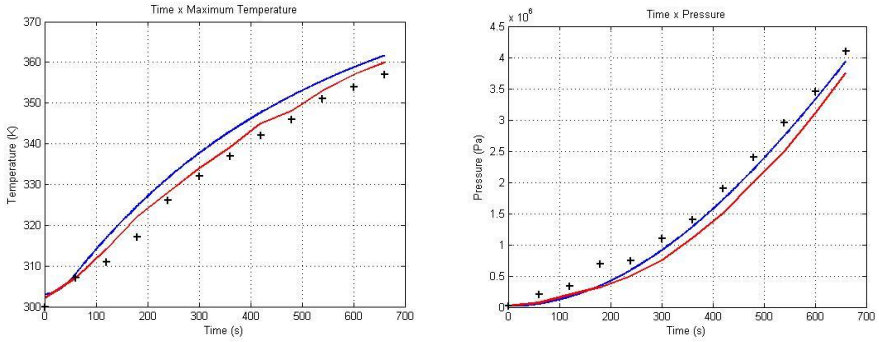

Figure 4. Validation Tests for 10 L/min. Blue: Simulations using FREEFEM++; Red: Numerical Simulations from (Sahoo,2011); Black Points: Experimental results from (Sahoo, 2011).

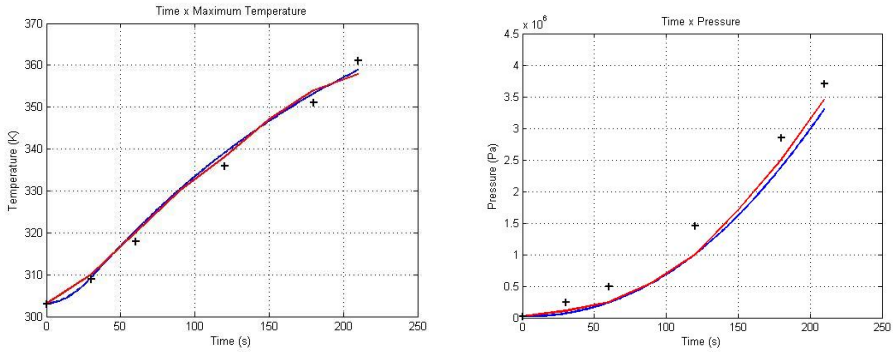

Figure 5. Validation Tests for 30 L/min. Blue: Simulations using FREEFEM++; Red: Numerical Simulations from [4]; Black Points: Experimental results from (Sahoo, 2011).

At $10L/min$, our values of pressure during the filling process are between the numerical and experimental results reported by (Sahoo, 2011). On considering $3.5MPa$ as the target pressure, our simulation achieved this value in 618 seconds, that is, 22s before that of the reference. Our values of maximum temperature were over those from (Sahoo, 2011). However, the maximum difference between numerical simulations was 4K. The results using $30L/min$ were closer to the literature than those for $10L/min$. The pressure achieved $3.5\ MPa$ in 215s, which is very close to numerical simulation of the reference ($3.5MPa$ in $212s$). The differences between the maximum temperatures were less than 1K, and the maximum temperature in 212s was 359.1K. The following figure illustrates the temperature evolution in our simulations, for both values of volumetric flow rate:

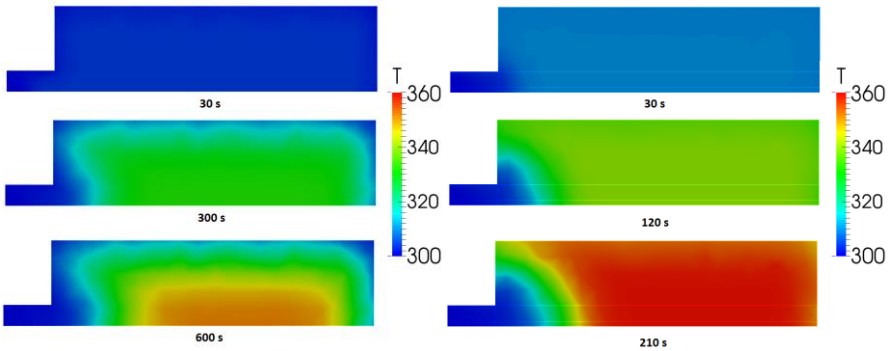

Figure 6. Temperature Distribution for different volumetric flows: Left: $10L/min$, Right: $30L/min$.

Despite the fact that values of maximum temperature at 3.5MPa were very close, the temperature distributions were different for distinct volumetric flow rates. The quantity of adsorbed gas was different too. The following figure presents the values of volumetric average density of adsorption at same pressures for both simulations:

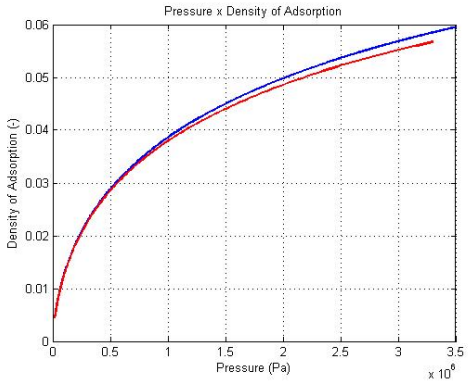

Figure 7. Average density of adsorption at different values of pressure. Blue: $10L/min$; Red: $30L/min$

As the pressure increases, the 10L/min simulation can store more adsorbed gas and the difference between the 30 L/min simulation also grows up. The reason for that could be seen in the fig. (6), where at the end of the filling process (600s and 210s respectively), the values of pressure are the same, but the temperature distributions are totally different. At $30L/min$, almost the whole volume was at temperatures that are close to 360K. On the other hand, the higher values of temperature in the simulation with $10L/min$ are located in a small region near the center of the tank. The major part is in "green", which represents temperatures close to 340K. This difference is also related to heat transfer through the tank walls. Both tests have the same ambient temperature, but the quantity of energy produced in the system is greater at $30L/min$, and it seems that there is not enough time to dissipate this amount of heat. The result is a rapid increase of the temperature. To put the difference in numbers, the density of adsorption is 3.1% greater at $10L/min$ in comparison with $30L/min$.

However, sometimes it could not be possible to reduce the volumetric flow, because the time of filling could be an important restriction. To increase the tank´s performance, keeping or rising the volumetric flow, a heat management is necessary to extract/insert heat produced/required in the adsorption/desorption process.

One possible solutions, presented in (Sahoo, 2011), proposes forced convection on the external walls of the tank. The authors changed the value of external heat transfer coefficient to $700\ W/m^2K$ and the density of adsorption after the filling process increased by 11.6%. However, most of adsorbents have low thermal conductivity and this solution is limited by this parameter. Figure (7) presents the comparison between temperature distributions with natural and forced convection:

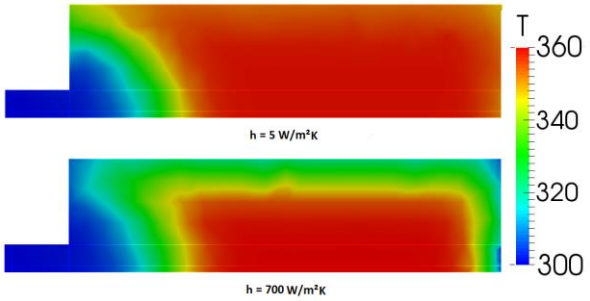

Figure 7. Temperature distribution for different values of external heat convection coefficient. ($30\ L/\mathrm{min}$)

Despite the increased the tank capacity, the forced convection has a limit on its influence inside the tank. To prove this assertion, the ideal process (isothermic in 300 K) could store 19.8% more adsorbed gas when compared to a tank with $h = 700\ W/m^2K$. This difference could be seen in fig. (7) when the regions with T = 300 K (blue) are located close to the inlet of the tank. The most of the tank have green color, owed to forced convection (T = 330 K) and red, with no influence of forced convection (T=350 K), remembering that density of adsorption reduces due to increase of temperature.

This article proposes a different approach to forced convection. The use of tubular heat exchangers with external natural convection and the results are present in the next section.

5. USE OF HEAT EXCHANGERS

One possible solution to increase the amount of gas inside the tank is active heat management during the filling process. Because of the limitations of the axisymmetric model, we considered only tubular heat exchangers positioned in radial direction. The tank geometry is the same as in the validation tests and the analysis was divided into two parts: Quantity

and position of tubes using the same tube diameter and with the best configuration found in theses tests, changing diameter and quantity of tubes while keeping the heat exchanger surface.
The first part consists in tanks with 5 mm diameter tubes, varying their quantity and position. To simplify the model, the temperature of the fluid inside the tubes was keep in 300 K in all tests and the coefficient of the heat transfer was 10 times that of the reference external forced convection test ($7000\ W/m^2K$). With these values, we can define a wall boundary condition for the heat exchanger. Natural convection conditions are imposed on the tank walls, because the objective here is to identify the performance of heat exchangers.
The following table presents the values for the tests that were performed. "Config" means tubes configuration either aligned (L) or tandem (T), R_i represents the radial position of the tubes relative to the center line of the tank, in mm, and Z_i is the axial position of the tubes in the same line, it is expressed in percents of L_2.

Table 5 – Heat Exchanger Tests – Same Diameter

Test	Config.	Matrix	R_1	R_2	R_3	Z_1	Z_2	Z_3	Z_4	Obs.
1	L	2x3	10	26	-	25	50	75	-	-
2	L	3x3	10	26	42	25	50	75	-	-
3	L	3x4	10	26	42	20	40	60	80	-
4	T	3x4	10	26	42	15	35	55	75	Line 1
						25	45	65	85	Line 2
						15	35	55	75	Line 3
5	T	3x4	10	26	42	25	45	65	85	Line 1
						15	35	55	75	Line 2
						25	45	65	85	Line 3

The fig. (8) presents to examples of geometry. A 2x3 aligned (L) and a 3x4 tandem (T):

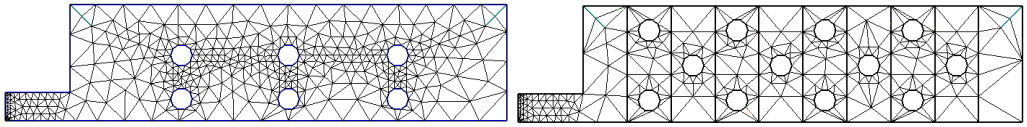

Figure 8. Mesh geometries to show the aligned and tandem configurations

The tests 1 and 2 had a low performance, with an increase close to 1.0% in tank capacity. This result could be explained by a trade-off between the reduction of available volume due to tubes (3.05% in test 1 and 6.47% in the test 2) and the gain of density of adsorption (5.33% and 10.09% respectively) in terms of reduction of the volume average temperature (342.4 K in test 1 and 334.8 K in test 2).
On the other hand, as the number of tubes increases, the density of adsorption also grows. These results concerning density of adsorption are an indication of the need to search the best position and the choice of a suitable diameter for the heat exchanger tubes.
In tests 3,4 and 5 we found an important consideration about the position of the tubes. The three cases had the same available volume and growth of density of adsorption in the tests with tandem configuration, as compared to aligned configuration. The growth of the density of adsorption in test 3 was 12.7% and in tests 4 and 5 it was 13.86 and 13,83% respectively. The average temperature in test 3 was close to 330 K, whereas tests 4 and 5 had the value close to 328 K.

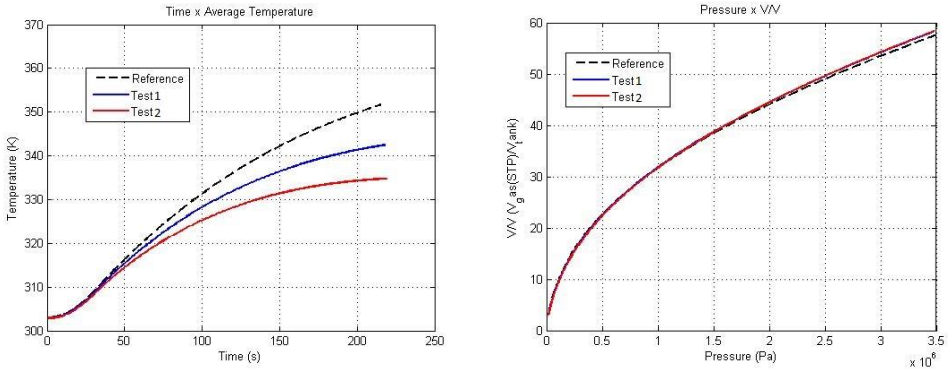

Figure 9. Results from tests 1 and 2: Left: Evolution of volumetric average temperature. Right: Evolution of V/V in terms of internal pressure.

Another way to present the results is by using the V/V parameter that was explained in the introduction. The reference simulation, with natural convection and without heat exchangers had V/V = 57.5. In the tests 1 and 2, the values are 1.0% greater as we mentioned previously. Tests 3,4 and 5 had better growth, with values achievering 58.6, 59.3 and 59.1 respectively.

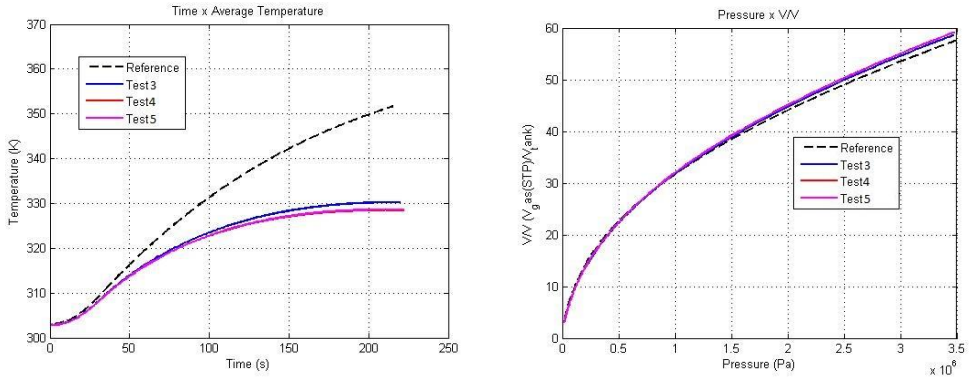

Figure 10. Results from tests 3,4 and 5: Left: Evolution of volumetric average temperature. Right: Evolution of V/V in terms of internal pressure.

To make clear the extent to which the heat exchangers have changed the temperature distribution, the following figure presents the results for tests 2,3,4 and 5:

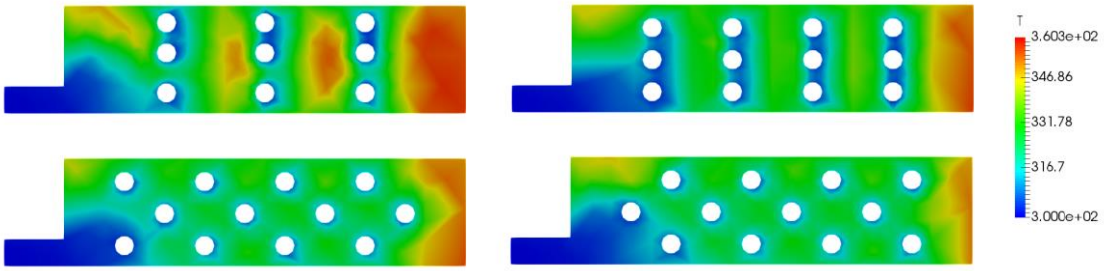

Figure 11. Temperature distribution for volumetric flow = 30 L/min. (Tests 2,3,4 and 5).

The green region grows up and occupies the most part of the tank, which increases the density of adsorption. The disposition of the tubes in the reservoir is crucial. Because in order to do a better configuration, less volume should be lost.

The second part of the tests adopts the same value of the surface area of the tests with 3x4 configurations, to generate two other geometries, as it is presented in the next tables. The diameters were 3.94 and 2.35 mm.

Table 6 – Heat Exchanger Test 6

T.	Config	M	R_1	R_2	R_3	R_4	Z_1	Z_2	Z_3	Z_4	Z_5	Obs.
6	T	4x5	10	20	30	40	5	25	45	65	85	Line 1
							15	35	55	75	95	Line 2
							5	25	45	65	85	Line 3
							15	35	55	75	95	Line 4

Table 7 – Heat Exchanger Test 7

T.	Config	M	R_1	R_2	R_3	R_4	R_5	R_6	Z_1	Z_2	Z_3	Z_4	Z_5	Obs.
7	T	6x5	8	16	24	32	40	48	5	25	45	65	85	Line 1
									15	35	55	75	95	Line 2
									5	25	45	65	85	Line 3
									15	35	55	75	95	Line 4
									5	25	45	65	85	Line 5
									15	35	55	75	95	Line 6

The results proved that diameter and position of the tubes are relevant in the search of optimal configurations. The internal volume of the test 6 was 1.68 L, more than tests 3,4 and 5 (1.67 L), but the V/V achieves 61.1 instead 59.1,

which represents an increase of 6.2% as compared to a tank without heat exchanger. Moreover, the average temperature reduced from 328K in tests 4 and 5 to 323 K in this test.

Better than the previous result, test 7 is assigned an internal volume of 1.73 L and the V/V reached 64.4, which represents an increase of 12.0% as compared to the baseline case, namely the tank without heat exchanger tubes. The average temperature has reduced to 318 K, the lowest of all tests. As a consequence, the highest increases in density of adsorption were found in these two tests. For test 6, the growth was 17.45% and for the test 10, the result achieved a 20.2% growth. The results showed the importance of a good choice of number, diameter and position of the tubes in the heat exchanger. There is a trade-off between the increase in tank capacity (measured by V/V) and the available volume inside the tank (which is reduced by the use of the device).

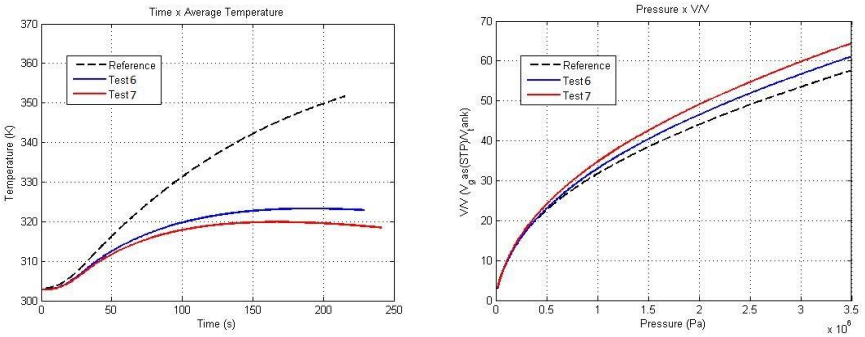

Figure 12. Results from tests 6 and 7: Left: Evolution of volumetric average temperature. Right: Evolution of V/V in terms of internal pressure.

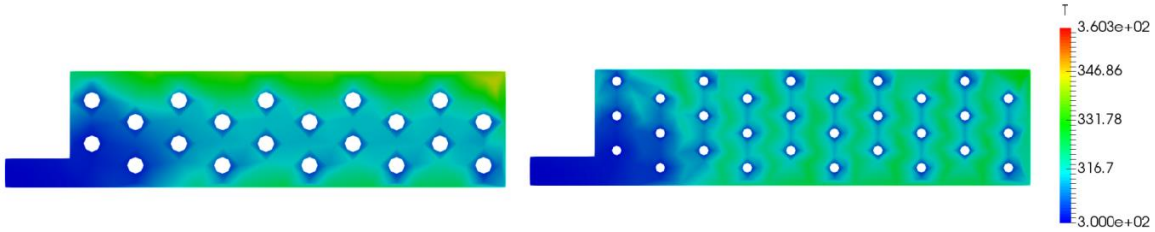

Figure 13. Temperature distribution for volumetric flow = 30 L/min. (Tests 6 and 7).

6. CONCLUSIONS

The results obtained in the validation tests proved that both the mathematical model and the numerical implementation can be used to simulate flow through porous media. After validating the solver, some exploratory tests, regarding the use of heat exchangers inside the tanks, were performed and showed that the use of these devices, while accounting for some parameters such as position of the tubes and their diameters, can increase the V/V relation and improve the capacity of storage of these tanks. The tubes that are arranged in tandem showed best results of V/V in comparison to aligned tubes, especially the test number 7, where the capacity of the tank increased more than 20% as compared to baseline test.

Although the results are good, there is still potential of increase the tank´s capacity because we did not explore all positions, diameters and quantity of tubes inside the tanks. The trade-off between the quantity of tubes and the available volume inside the tank is an important parameter to find the best configurations.

To tackle this problem, an optimization method will be necessary and this is the next step of this work. We plan to make use the so-called Adjoint Method to estimate the sensitivity gradient of a given objective function and to use this information in an optimization loop.

This method will be also programmed in FREEFEM++ platform, thus creating an optimization loop in the same source code. That is the reason why we prefer to program the governing equations in the same platform rather than to use commercial software, such as FLUENT and COMSOL MULTPHYSICS where the software integration could take some fine tunning.

7. ACKNOWLEDGMENTS

The authors gratefully acknowledge support from Shell and FAPESP through the “Reserch Centre for Gas Innovation - RCGI” (Fapesp Proc. 2014/50279-4), hosted by the University of Sao Paulo, and the strategic importance of the support given by ANP (Brazil’s National Oil, Natural Gas and Biofuels Agency) through the R&D levy regulation."

8. REFERENCES

CIA The World Factbook - https://www.cia.gov/library/publications/theworld-factbook/rankorder/2253rank.html. [S.l.]: US Goverment, 2016.

JUDD, R. W.; GLADDDING, R. e. a. The use of adsorbed natural gas technology for large scale storage. BG Technology, Gas research and Technology Centre., 1998.

RAHMAN, K. Experimental and Theoretical Studies on Adsorbed Natural Gas Storage System using Activated Carbons. Tese (Doutorado) _ National University of Singapore, 2011.

SAHOO, P.; JOHN, M. e. a. Filling characteristics for an activated carbon based adsorbed natural gas storage system. I & EC research, 2011.

MOTA, J.; SAATDJIAN, E. e. a. A simulation model of high capacity methane adsorptive storage system. Adsorption 1, 1995.

HECHT, F.; New development in FreeFem++. Journal of Numerical Mathematics, 2012, no 3-4, 251-265

HIRATA, S. COUTO, P. Modeling and hybrid simulation of slow discharge process of adsorbed methane tanks. International Journal of Thermal Sciences, 2009.

9. RESPONSIBILITY NOTICE

The authors are the only responsible for the printed material included in this paper.